J Biomol NMR (2014) 60:265–274
DOI 10.1007/s10858-014-9873-8

ARTICLE

A 3D time-shared NOESY experiment designed to provide optimal resolution for accurate assignment of NMR distance restraints in large proteins

Subrata H. Mishra · Bradley J. Harden · Dominique P. Frueh

Received: 16 September 2014 / Accepted: 31 October 2014 / Published online: 9 November 2014

Abstract Structure determination of proteins by solution NMR has become an established method, but challenges increase steeply with the size of proteins. Notably, spectral crowding and signal overlap impair the analysis of cross-peaks in NOESY spectra that provide distance restraints for structural models. An optimal spectral resolution can alleviate overlap but requires prohibitively long experimental time with existing methods. Here we present a time-shared 3D experiment optimized for large proteins that provides ^{15}N and ^{13}C dispersed NOESY spectra in a single measurement. NOESY correlations appear in the detected dimension and hence benefit from the highest resolution achievable of all dimensions without increase in experimental time. By design, this experiment is inherently optimal for non-uniform sampling acquisition when compared to current alternatives. Thus, ^{15}N *and* ^{13}C dispersed NOESY spectra with ultra-high resolution in all dimensions were acquired in parallel within about 4 days instead of 80 days for a 52 kDa monomeric protein at a concentration of 350 μM.

Keywords Large proteins · Resolution · TROSY NOESY · NMR structure determination · Time-shared

Electronic supplementary material The online version of this article (doi:10.1007/s10858-014-9873-8) contains supplementary material, which is available to authorized users.

S. H. Mishra · B. J. Harden · D. P. Frueh (✉)
Department of Biophysics and Biophysical Chemistry, Johns Hopkins University School of Medicine, 701 Hunterian, 725 North Wolfe St., Baltimore, MD 21205, USA
e-mail: dfrueh@jhmi.edu

Introduction

Over the years, nuclear magnetic resonance has become a mainstay of protein structural studies as it allows structure determination both in the presence of molecular motions and at near physiological conditions. Structure determinations by solution NMR predominantly rely on 3D NOESY spectra to provide inter-proton distance restraints. These restraints are obtained from the intensity of cross-peak signals in NOESY spectra that report on nuclei that are spatially close. Thus, the accuracy of NMR structures depends on the *completeness* and *accuracy* of NOESY cross-peak assignments. In large proteins, both rapid transverse relaxation and spectral crowding impede proper assignment. Rapid transverse relaxation leads to weak and broad NMR signals; it is minimized to a large extent by the combination of transverse relaxation optimized spectroscopy (TROSY) (Pervushin et al. 1997) and deuteration (Gardner and Kay 1998). However, uniform incorporation of deuterons removes probes necessary for NMR structure determination. Hence, to combat relaxation while maintaining structural probes, samples are selectively protonated and ^{13}C enriched for a subset of methyl moieties (e.g. for Ile (δ_1), Leu, Val, Ala) in an otherwise uniform ^{15}N–^{2}H–^{12}C background (Gardner and Kay 1998; Goto et al. 1999; Goto and Kay 2000; Isaacson et al. 2007; Ayala et al. 2009). Thus, only methyl and amide protons (reintroduced by exchange with H_2O solvent) are detected. In principle, such a labeling scheme (e.g. ILV or ILVA labeling) alleviates spectral crowding and provides narrower signals. However, in practice, resolving such narrow signals is limited by the digital resolution of the spectra, which for indirect dimensions in NMR spectra is limited by experimental time. That is, the ability to identify correlations is no longer limited by relaxation and line-broadening

but instead by the time necessary to achieve a resolution sufficient to resolve signals. Current 3D NOESY experiments designed for large proteins are ill-equipped to overcome this obstacle.

Here, we combine three strategies to provide ultra-high resolution 3D NOESY spectra within a conventional acquisition time. First, a novel time-shared strategy provides HC-HSQC-NOESY and HN-TROSY-NOESY spectra simultaneously with minimal losses in sensitivity. The savings in experimental time can then be reinvested in improving spectral resolution. Second, NOESY cross-peaks are featured along the detected dimension, as opposed to the indirect dimension in current time-shared 3D NOESY experiments. Therefore, the signals benefit from the detected dimension's intrinsically high resolution at no cost in experimental time. Finally, we show that the experiment is inherently optimal for accelerated data acquisition using non-uniform sampling in the indirect dimensions. In the end, a single acquisition provides two 3D spectra of unparalleled resolution in all dimensions within $\sim$4 days. The advantages of this experiment are demonstrated with a 350 μM, ILV labeled sample of a nonribosomal peptide synthetase heterocyclization domain, a 52 kDa monomeric protein.

Materials and methods

Cloning, expression and purification of Cy1

All experimental data were recorded on a 52 kDa cyclization domain (Cy1) from the HMWP2 subunit of the *Yersinia pestis* yersiniabactin synthetase (Keating et al. 2000). The $\sim$1.4 kb fragment encompassing the Cy1 domain (residues 101–544) was amplified from pHMWP2.CH8 (Keating et al. 2000) (a gift from Christopher Walsh's lab, Harvard Medical School) ligated into the pET30a expression vector (Novagen, San Diego, CA) and transformed into *E. coli* BL21(DE3) cells (Novagen). This construct expresses the Cy1 protein with LE-HHHHHH appended to the C-terminus (construct named Cy1H6).

The NMR sample used in our studies is uniformly labeled with ^{2}H, ^{15}N, and ^{12}C, while the methyl groups of Ile (δ_1 position only), Leu and Val side-chains are labeled with ^{1}H and ^{13}C. Phe and Tyr residues are protonated and enriched in ^{15}N (Muchmore et al. 1989; Gross et al. 2003). BL21(DE3) cells with the pET30a-Cy1H6 plasmid were initially grown in an overnight 50 mL LB medium at 37 °C (250 rpm). 1 mL overnight culture was used to inoculate 1 L of M9 minimal medium (6 g/L Na_2HPO4, 3 g/L KH_2PO_4, 0.5 g/L NaCl, 2 mM $MgCl_2$, 0.1 mM $CaCl_2$) in 99.9 % D_2O (Sigma/Aldrich) containing 2 g/L ^{2}H glucose (Cambridge Isotope Laboratories, CIL), 1 g/L $^{15}NH_4Cl$ (Sigma/Aldrich), 10 mL vitamin solution (0.5 g/L thiamine, 0.1 g/L D-biotin, 0.1 g/L choline chloride, 0.1 g/L folic acid, 0.1 g/L niacinamide, 0.1 g/L D-pantothenic acid, 0.1 g/L pyridoxal and 0.01 g/L riboflavin, in 99.9 % D_2O), 2 mL of trace element solution (in 99.9 % D_2O) (Cai et al. 1998), and 50 mg/L kanamycin. At $O.D._{600} \sim 0.5$, 75 mg of ^{13}C-methyl-α-ketobutyrate (CIL), 125 mg of $^{13}C_2$-dimethyl-α-ketoisovalerate (CIL), 150 mg of ^{15}N-Tyrosine (CIL), and 150 mg of ^{15}N-Phenylalanine (CIL) were added. Once $O.D._{600}$ reached about 0.6, cells were chilled to about 16 °C (ice bath), and protein expression was induced with 0.5 mM IPTG for an additional 12 h (16 °C × 250 rpm) until an $O.D._{600}$ of approximately 1.4 was reached. Cell pellets were harvested by centrifugation (4 °C, 5,000×*g*, 20 min) and were kept at −80 °C until further use. Cell pellets were thawed on ice and re-suspended in 50 mL of chilled lysis buffer (50 mM Tris, pH 8 at 4 °C, 0.1 M NaCl, 5 mM Imidazole, 5 mM β-mercaptoethanol, 100 μg/mL Lysozyme, 50 μg/mL DNase I). All buffers used in the purification protocol were filtered with a 0.22 μm filter and degassed for 20 min before use. Cells were lysed with a microfluidizer (Microfluidics Inc. Waltham, MA) and cellular debris pelleted by centrifugation (4 °C, 15,000×*g*, 30 min) followed by filtration using a 0.22 μm filter. The filtered lysate was loaded onto a 5 mL HisTrap HP column (GE Healthcare, Sweden) pre-equilibrated with His-Buffer A (50 mM Tris, pH 8 at 4 °C, 0.5 M NaCl, 5 mM Imidazole, 5 mM β-mercaptoethanol). The HisTrap column was washed with 100 mL of His-Buffer A at 4 mL/min after loading the lysate, and Cy1H6 was then eluted by a 0–100 % gradient of His-Buffer B (50 mM Tris, pH 8 at 4 °C, 0.5 M NaCl, 0.5 M Imidazole, 5 mM β-mercaptoethanol) at a flow rate of 3 mL/min. Fractions containing Cy1H6 (confirmed by SDS-PAGE) were pooled and dialyzed overnight at 4 °C against the dialysis buffer (50 mM Tris, pH 8 at 4 °C, 0.1 M NaCl, 20 mM β-mercaptoethanol, 1 mM EDTA). The dialysate was filtered (0.22 μm filter) and concentrated at 4,000×*g* and 4 °C to $\sim$3 mL using an Amicon Ultra centrifugal filter (10,000 NMWL, Millipore, Ireland). The concentrated solution was injected in 1 mL batches onto a size exclusion chromatography (SEC) column (16/60 Superdex 75 column, GE Healthcare) equilibrated with SEC buffer (20 mM Sodium Phosphate buffer, 100 mM NaCl, 1 mM EDTA, 5 mM DTT, pH 7) at 0.7 ml/min. The single mono dispersed peak containing Cy1H6 ($\varepsilon_{280} = 88{,}265\ M^{-1}\ cm^{-1}$) was then concentrated and buffer exchanged into the NMR buffer (20 mM Sodium Phosphate, 10 mM NaCl, 1 mM EDTA, 5 mM DTT, pH 7.0) using 10,000 NMWL Amicon Ultra centrifugal filters (4 °C, 2,000×*g*). The final NMR sample contained 5 % D_2O and the final protein concentration was 350 μM.

Acquisition and processing

All NMR experiments were conducted at 25 °C on a Bruker 600 MHz AVANCE III spectrometer equipped with a QCI cryoprobe™. Both 3D TS-HN-TROSY/HC-HSQC-NOESY (TS-TR/HS-NO) and TS-NOESY-HN-TROSY/HC-HSQC (TS-NO-TR/HS, see supplementary information S4) spectra (Fig. 2) were acquired with 512 (^{1}H detected) × 150 (^{1}H indirect) × 30 (^{15}N/^{13}C indirect) complex points. The spectral widths in the detected ^{1}H and indirect ^{15}N/^{13}C dimensions were 16 and 35/24 ppm, respectively. The indirect ^{1}H dimension had a spectral width of 13 ppm for the TS-NO-TR/HS and 6.5 ppm for the TS-TR/HS-NO. The TS-NO-TR/HS was acquired with 16 scans per quadrature component ($R(t_1)R(t_2)$, $I(t_1)R(t_2)$, $R(t_1)I(t_2)$, $I(t_1)I(t_2)$). For the TS-TR/HS-NO, 16 repetitions of the experiment were stored individually with each accumulating 4 scans. After processing (see below), both TS-NO-TR/HS and TS-TR/HS-NO have the equivalent of 16 scans per quadrature component. A recycle delay of 1 s was used for both experiments. The acquisition times were 4 days, 7 h, 2 min for TS-TR/HS-NO and 4 days, 7 h, 16 min for TS-NO-TR/HS.

The TS-TR/HS-NO data is initially processed with a python script (available from the corresponding author upon request) which adds and subtracts interleaved acquisitions to separate the ^{15}N and ^{13}C pathways, recombines the transients according to Tables 3 and 4 ("Results and discussion" section), and rearranges the data so that traditional NMRPipe (Delaglio et al. 1995) scripts can be used for processing (using the complex flag).

Both TS datasets, TS-TR/HS-NO and TS-NO-TR/HS, were processed with the same cosine-squared bell apodization functions for the respective dimensions. Linear prediction was used to double the number of points in the indirect dimensions, which were subsequently zero-filled to 256 and 512 points in the ^{15}N/^{13}C and ^{1}H dimensions, respectively. The detected dimensions were zero-filled to 1,024 points before being Fourier transformed. NMRPipe (Delaglio et al. 1995) scripts were used to perform all the spectral processing mentioned above. All strips and overlays displayed in Figs. 2 and 3 were created in CARA (Keller 2003). Peak Picking in each spectrum was performed using the program NMRDraw.

The non-uniformly sampled TS-TR/HS-NO spectra in Fig. 3 were collected in the same time frame (4 days, 4 h, 48 min) and had the same spectral widths and acquisition parameters as its uniformly sampled counterpart. A sampling schedule spanning 45,000 complex points (150 ^{15}N/^{13}C × 300 ^{1}H complex points) with a sampling factor of 10 % was generated with the software PoissonGap (Hyberts et al. 2012). The seed used to generate the schedule was 12321. The TR-NO and HS-NO datasets were separated using the python script mentioned earlier and the indirect dimensions were reconstructed using the iterative soft thresholding software hmsIST (Hyberts et al. 2012) using 500 iterations per plane. Linear prediction was not used for the indirect dimensions. Apodization and zero-filling in the direct and indirect dimensions were performed as in the uniformly acquired dataset.

Results and discussion

Time-shared NOESY pulse sequence

Time-shared (TS) experiments allow simultaneous acquisition of spectra involving different nuclei that would otherwise require individual measurements (Farmer II 1991; Boelens et al. 1994; Sattler et al. 1995). TS acquisition is only beneficial when sensitivity losses in the resulting spectra do not exceed 40 % compared to those obtained sequentially. Thus, time-shared coherence transfers must be efficient for both nuclei and the experiment must minimize additional spin manipulations when compared to individual experiments. Würtz et al. (2007) have shown that the optimal TS back-transfer for methyl and amide groups combines a simple HSQC (Bodenhausen and Ruben 1980) with the so-called planar mixing HN-TROSY implementation (Yang and Kay 1999; Nietlispach 2005). The planar mixing HN-TROSY implementation offers higher sensitivity (Yang and Kay 1999) than the ST2-PT scheme (Pervushin et al. 1998) for amide moieties, and in TS implementation, it allows methyl proton magnetization to be stored longitudinally for a substantial period, thereby minimizing losses stemming from relaxation (Würst et al. 2007). However, in the TS experiment of Würst et al., amide proton detection is performed by gradient selection in contrast to methyl protons. Therefore, simultaneous detection of amide and methyl signals *requires* long selective pulses and a number of compensation periods. Similar constraints also occur when pairing an HN-TROSY with an HC-HMQC. In general, spin manipulations that are selective to a single pathway lead to sensitivity reduction for both amide and methyl signals due to transverse relaxation, a common problem in TS experiments (Frueh et al. 2006; Guo and Tugarinov 2009). Hence, in order to maximize sensitivity, we designed a novel TS block pairing an HC-HSQC with a novel planar mixing HN-TROSY scheme employing phase cycling rather than gradient selection. Our phase-cycled scheme enables simultaneous detection of amide and methyl proton signals in TS experiments without additional spin manipulations. Addition of a NOESY block following our TS scheme yields the 3D TS-HN-TROSY/HC-HSQC-NOESY (TS-TR/HS-NO) experiment (Fig. 1) featuring nOe correlations in the direct

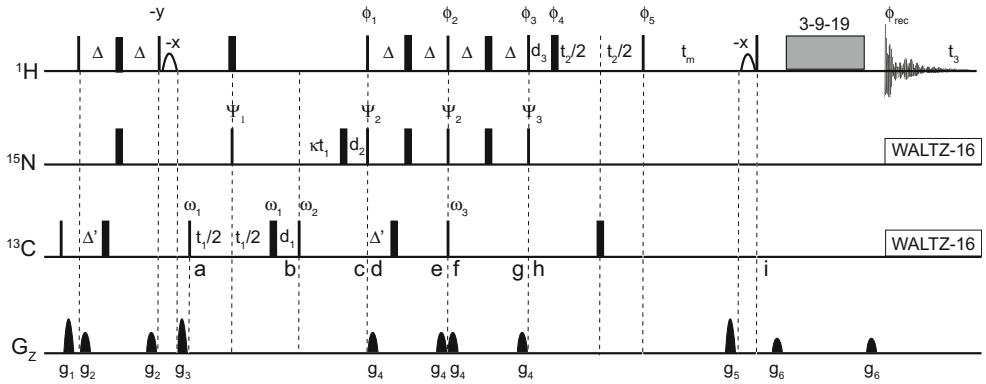

Fig. 1 Pulse sequence of the 3D TS-HN-TROSY/HC-HSQC-NOESY experiment. *Narrow* and *wide bars* represent 90° and 180° hard pulses, respectively. All pulses are applied along the x axis unless mentioned otherwise. The *empty ellipsoids* represent water-selective 90° rectangular pulses. The block labeled 3-9-19 is a WATERGATE water suppression scheme (Piotto et al. 1992). The delays are $\Delta = 1/(4J_{NH})$, $\Delta' = 1/(4J_{CH})$ and, $t_m = 150$ ms (mixing time). The delays $d_1 = pw_N$, $d_2 = 3 * pw_C + pw_N$, and $d_3 = 2 * pw_C$ are used to prevent first order phase corrections in indirect dimensions; pw_C and pw_N are the 90° pulse widths for ^{13}C and ^{15}N nuclei, respectively. The time-shared evolution of ^{15}N and ^{13}C coherences has been implemented as published previously (Würtz et al. 2007). $\kappa = SW(C)/SW(N) - ½$ with SW(C) and SW(N) the spectral widths of ^{13}C (24 ppm) and ^{15}N (35 ppm), respectively. The filled ellipsoids (line labeled G_z) are 1 ms smoothed-square shaped-pulse gradients: $g_1 = -36$ G/cm, $g_2 = 7.5$ G/cm, $g_3 = 25.5$ G/cm, $g_4 = 2.5$ G/cm, $g_5 = -40$ G/cm and $g_6 = 4$ G/cm; each gradient pulse is followed by a 200 µs recovery delay. ^{13}C and ^{15}N decoupling during detection are both achieved using WALTZ-16 sequences (Shaka et al. 1983), with field strengths of 0.71 kHz. Simultaneous ^{13}C and ^{15}N decoupling necessitates the use of lower field strengths and synchronous pulsing to prevent artifacts (Van Ingen et al. 2002). The pulse phases detailed henceforth are spin-dynamic phases and should be modified appropriately depending on the NMR spectrometer used (Roehrl et al. 2005). Spin state selection (^{15}N) and quadrature detection in both indirect dimensions (t_1 & t_2) is achieved by post-acquisition combinations of transients that are recorded and stored separately. These transients have the following phase settings: A1: $\phi_1 = y$, $\phi_2 = x$, $\phi_3 = -x$, $\psi_1 = y\ -y$, $\psi_2 = -y$, $\psi_3 = x$, $\omega_1 = x\ -x$, $\omega_2 = x$, $\omega_3 = x\ \ x\ -x\ -x$; A2: $\phi_1 = x$, $\phi_2 = y$, $\phi_3 = -y$, $\psi_1 = y\ -y$, $\psi_2 = -x$, $\psi_3 = y$, $\omega_1 = y\ -y$, $\omega_2 = x$, $\omega_3 = x\ \ x\ -x\ -x$; A3: $\phi_1 = y$, $\phi_2 = x$, $\phi_3 = x$, $\psi_1 = y\ -y$, $\psi_2 = -y$, $\psi_3 = x$, $\omega_1 = x\ \ -x$, $\omega_2 = x$, $\omega_3 = x\ \ x\ -x\ -x$; A4: $\phi_1 = x$, $\phi_2 = y$, $\phi_3 = y$, $\psi_1 = y\ -y$, $\psi_2 = -x$, $\psi_3 = y$, $\omega_1 = y\ -y$, $\omega_2 = x$, $\omega_3 = x\ x\ -x\ -x$. $\phi_{rec} = x\ -x\ x\ -x$, for all transients. It should be noted that the 4-step phase cycle in each transient is used to remove artifacts and not for quadrature detection and line-selection. A1–A4 are recorded either with $\phi_4 = -y$ and $\phi_5 = x$ ($A1_x$–$A4_x$) or with $\phi_4 = x$ and $\phi_5 = y$ ($A1_y$–$A4_y$), where the subscript denotes the phase of ϕ_5. To delineate ^{15}N and ^{13}C edited spectra, these 8 transients are recorded a second time with the phase of ω_2 inverted. TPPI (Marion and Wuthrich 1983) is implemented during t_1 evolution using the phases ψ_1, ω_1 and ϕ_{rec}. The 90° ^{13}C pulse applied at point d is used to cancel weak dispersive artifacts which result from incomplete conversion of strong methyl proton antiphase coherences into in-phase coherences in the period b to c. All experiments were conducted at 25 °C on a 600 MHz Bruker Avance III spectrometer equipped with a CP-QCI ^{1}H/^{31}P/^{13}C/^{15}N–^{2}H cryoprobe™ with a single axis gradient coil. Both Bruker and Agilent pulse programs can be obtained by contacting the corresponding author

dimension. In the end, our 3D TS-TR/HS-NO experiment provides a 3D-HN-TROSY-NOESY (TR-NO) with no detected loss in sensitivity and a 3D-HC-HSQC-NOESY (HS-NO) with only 21 % loss in sensitivity when each spectrum is compared to that of an individual experiment (supplementary information S2).

The pulse sequence uses a time-shared INEPT element (Farmer II 1991; Boelens et al. 1994) to convert amide and methyl proton polarizations into ^{15}N and ^{13}C single-quantum coherences (SQCs), respectively (Fig. 1a). Using the scheme designed by Würtz et al., ^{15}N SQCs evolve during t_1 with attenuated transverse relaxation while evolution under $^1J_{CH}$ scalar couplings is refocused for ^{13}C SQCs. Next, ^{15}N and ^{13}C coherences are simultaneously converted back to ^{1}H coherences using our HN-TROSY scheme (Fig. 1d–h; Table 1) paired with a reverse HC-INEPT scheme (Fig. 1d–e). As in the experiment by Würtz et al., methyl magnetization is stored longitudinally during the second half of the HN-TROSY scheme (Fig. 1f–g; Table 1) to minimize signal losses. Table 1 displays the density operator elements present throughout the time-shared transfer (Fig. 1c–h). Methyl and amide proton chemical shifts are encoded during t_2 (Fig. 1h) followed by a mixing period (t_m) and finally, at point i, a 3-9-19 water-suppression scheme is applied before detection. The amide and methyl proton coherences encoded with t_1 and t_2 evolutions are listed in the supplementary information (S3). Amide and methyl signals are separated during processing by addition and subtraction of interleaved acquisitions recorded with opposite phases of ω_2, which only inverts the phase of the methyl signals (Frueh et al. 2006).

Sensitivity enhancement and spin-state selection for amide groups and quadrature detection for all indirect dimensions are all achieved simultaneously with an unconventional data acquisition scheme. Eight transients with different phase settings ($A1_x$–$A4_x$ and $A1_y$–$A4_y$,

Table 1 Amide (HN-TROSY) and methyl (HC-HSQC) coherences at points c through h for the TS-TR/HS-NO pulse sequence in Fig. 1

	c	d	e	f	g	h	
HN-TROSY							
A1	$-2\ ^{N}H_zN_x$	$2\ ^{N}H_xN_z$	$^{N}H_y$	$^{N}H_z$	$-^{N}H_z$	$-^{N}H_y$	$½\ (c_N^+ c_{\bar{N}})$
	$-N_y$	$-N_y$	$2\ ^{N}H_zN_x$	$2\ ^{N}H_yN_z$	$^{N}H_x$	$^{N}H_x$	$½\ (s_N^+ - s_{\bar{N}})$
	$-2\ ^{N}H_zN_y$	$-2\ ^{N}H_xN_y$	$2\ ^{N}H_xN_y$	$2\ ^{N}H_xN_y$	$-2\ ^{N}H_xN_y$	$2\ ^{N}H_xN_z$	$½\ (s_N^+ + s_{\bar{N}})$
	N_x	$-N_z$	N_z	N_x	$-2\ ^{N}H_zN_y$	$2\ ^{N}H_yN_z$	$½\ (c_{\bar{N}} - c_N^+)$
A2	$-2\ ^{N}H_zN_x$	$2\ ^{N}H_yN_x$	$-2\ ^{N}H_yN_x$	$-2\ ^{N}H_yN_x$	$2\ ^{N}H_yN_x$	$2\ ^{N}H_yN_z$	$½\ (c_N^+ + c_{\bar{N}})$
	$-N_y$	$-N_z$	N_z	$-N_y$	$2\ ^{N}H_zN_x$	$-2\ ^{N}H_xN_z$	$½\ (s_N^+ - s_{\bar{N}})$
	$-2\ ^{N}H_zN_y$	$2\ ^{N}H_yN_z$	$^{N}H_x$	$-^{N}H_z$	$^{N}H_z$	$-^{N}H_x$	$½\ (s_N^+ + s_{\bar{N}})$
	N_x	N_x	$-2\ ^{N}H_zN_y$	$-2\ ^{N}H_xN_z$	$-^{N}H_y$	$-^{N}H_y$	$½\ (c_{\bar{N}} - c_N^+)$
A3	$-2\ ^{N}H_zN_x$	$2\ ^{N}H_xN_z$	$^{N}H_y$	$^{N}H_z$	$-^{N}H_z$	$^{N}H_y$	$½\ (c_N^+ + c_{\bar{N}})$
	$-N_y$	$-N_y$	$2\ ^{N}H_zN_x$	$2\ ^{N}H_yN_z$	$^{N}H_x$	$^{N}H_x$	$½\ (s_N^+ - s_{\bar{N}})$
	$-2\ ^{N}H_zN_y$	$-2\ ^{N}H_xN_y$	$2\ ^{N}H_xN_y$	$2\ ^{N}H_xN_y$	$-2\ ^{N}H_xN_y$	$2\ ^{N}H_xN_z$	$½\ (s_N^+ + s_{\bar{N}})$
	N_x	$-N_z$	N_z	N_x	$-2\ ^{N}H_zN_y$	$-2\ ^{N}H_yN_z$	$½\ (c_{\bar{N}} - c_N^+)$
A4	$-2\ ^{N}H_zN_x$	$2\ ^{N}H_yN_x$	$-2\ ^{N}H_yN_x$	$-2\ ^{N}H_yN_x$	$2\ ^{N}H_yN_x$	$2\ ^{N}H_yN_z$	$½\ (c_N^+ + c_{\bar{N}})$
	$-N_y$	$-N_z$	N_z	$-N_y$	$2\ ^{N}H_zN_x$	$2\ ^{N}H_xN_z$	$½\ (s_N^+ - s_{\bar{N}})$
	$-2\ ^{N}H_zN_y$	$2\ ^{N}H_yN_z$	$^{N}H_x$	$-^{N}H_z$	$^{N}H_z$	$^{N}H_x$	$½\ (s_N^+ + s_{\bar{N}})$
	N_x	N_x	$-2\ ^{N}H_zN_y$	$-2\ ^{N}H_xN_z$	$-^{N}H_y$	$-^{N}H_y$	$½\ (c_{\bar{N}} - c_N^+)$
HC-HSQC							
A1	$2\ ^{C}H_zC_z$	$2\ ^{C}H_xC_z$	$-^{C}H_y$	$-^{C}H_z$	$^{C}H_z$	$^{C}H_y$	$\cos(\omega_C t_1)$
A2	$-2\ ^{C}H_zC_z$	$2\ ^{C}H_yC_z$	$-^{C}H_x$	$^{C}H_z$	$-^{C}H_z$	$^{C}H_x$	$\sin(\omega_C t_1)$
A3	$2\ ^{C}H_zC_z$	$2\ ^{C}H_xC_z$	$-^{C}H_y$	$-^{C}H_z$	$^{C}H_z$	$-^{C}H_y$	$\cos(\omega_C t_1)$
A4	$-2\ ^{C}H_zC_z$	$2\ ^{C}H_yC_z$	$-^{C}H_x$	$^{C}H_z$	$-^{C}H_z$	$-^{C}H_x$	$\sin(\omega_C t_1)$

J_{NH} is the coupling constant between amide protons and nitrogens. The negative sign of the ^{15}N gyromagnetic ratio and $J_{NH} < 0$ was accounted for in all calculations. $c_N^+ = \cos[(\omega_N + \pi J_{NH})t_1]$, $c_{\bar{N}} = \cos[(\omega_N - \pi J_{NH})t_1)]$, $s_N^+ = \sin[(\omega_N + \pi J_{NH})t_1]$, and $s_{\bar{N}} = \sin[(\omega_N - \pi J_{NH})t_1]$. $½\ (c_N^+ c_{\bar{N}}) = \cos(\omega_N t_1)\cos(\pi J_{NH} t_1)$, etc. ω_N and ω_C are the amide nitrogen and methyl carbon frequencies respectively encoded during t_1 evolution. ^{N}H and ^{C}H refer to amide and methyl proton coherences respectively. Only operators that contribute to observable signals are shown

Table 2 Transients recorded before separation of amide and methyl signals

	Transients recorded
$A1_x$	$S_N\, e^{(-i\omega_H t_3)}\,(c_N^+ c_{HN}^- - s_N^+ s_{HN}^- + c_{\bar{N}} c_{HN}^+ + s_{\bar{N}} s_{HN}^+) - S_c\, e^{(-i\omega_H t_3)} \cos(\omega_C t_1) \cos(\omega_{HC} t_2)$
$A2_x$	$S_N\, e^{(-i\omega_H t_3)}\,(-c_N^+ c_{HN}^- + s_N^+ s_{HN}^- + c_{\bar{N}} c_{HN}^+ + s_{\bar{N}} s_{HN}^+) - S_c\, e^{(-i\omega_H t_3)} \sin(\omega_C t_1) \sin(\omega_{HC} t_2)$
$A3_x$	$S_N\, e^{(-i\omega_H t_3)}\,(-c_N^+ c_{HN}^- - s_N^+ s_{HN}^- - c_{\bar{N}} c_{HN}^+ + s_{\bar{N}} s_{HN}^+) + S_c\, e^{(-i\omega_H t_3)} \cos(\omega_C t_1) \cos(\omega_{HC} t_2)$
$A4_x$	$S_N\, e^{(-i\omega_H t_3)}\,(-c_N^+ c_{HN}^- - s_N^+ s_{HN}^- + c_{\bar{N}} c_{HN}^+ - s_{\bar{N}} s_{HN}^+) + S_c\, e^{(-i\omega_H t_3)} \sin(\omega_C t_1) \sin(\omega_{HC} t_2)$
$A1_y$	$S_N\, e^{(-i\omega_H t_3)}\,(c_N^+ s_{HN}^- + s_N^+ c_{HN}^- + c_{\bar{N}} s_{HN}^+ - s_{\bar{N}} c_{HN}^+) - S_c\, e^{(-i\omega_H t_3)} \cos(\omega_C t_1) \sin(\omega_{HC} t_2)$
$A2_y$	$S_N\, e^{(-i\omega_H t_3)}\,(-c_N^+ s_{HN}^- - s_N^+ c_{HN}^- + c_{\bar{N}} s_{HN}^+ - s_{\bar{N}} c_{HN}^+) + S_c\, e^{(-i\omega_H t_3)} \sin(\omega_C t_1) \cos(\omega_{HC} t_2)$
$A3_y$	$S_N\, e^{(-i\omega_H t_3)}\,(-c_N^+ s_{HN}^- + s_N^+ c_{HN}^- - c_{\bar{N}} s_{HN}^+ - s_{\bar{N}} c_{HN}^+) + S_c\, e^{(-i\omega_H t_3)} \cos(\omega_C t_1) \sin(\omega_{HC} t_2)$
$A4_y$	$S_N\, e^{(-i\omega_H t_3)}\,(-c_N^+ s_{HN}^- + s_N^+ c_{HN}^- + c_{\bar{N}} s_{HN}^+ + s_{\bar{N}} c_{HN}^+) - S_c\, e^{(-i\omega_H t_3)} \sin(\omega_C t_1) \cos(\omega_{HC} t_2)$

A1–A4 are recorded with $\phi_5 = x$ ($A1_x$–$A4_x$) and $\phi_5 = y$ ($A1_y$–$A4_y$), where the subscript denotes the phase of ϕ_5. S_N and S_C are the amplitudes of the detected amide and methyl proton signals respectively, and ω_H is the frequency of the NOESY cross-peak encoded in the detected proton dimension (t_3). c_N^+, $c_{\bar{N}}$, s_N^+, and $s_{\bar{N}}$ are described in Table 1. $c_{HN}^+ = \cos[(\omega_{HN} + \pi J_{NH})t_2]$, $c_{HN}^- = \cos[(\omega_{HN} - \pi J_{NH})t_2]$, $s_{HN}^+ = \sin[(\omega_{HN} + \pi J_{NH})t_2]$, $s_{HN}^- = \sin[(\omega_{HN} - \pi J_{NH})t_2]$. ω_{HN} and ω_{HC} are the amide proton and methyl proton frequencies encoded during t_2 evolution. The negative sign of the ^{15}N gyromagnetic ratio and $J_{NH} < 0$ was accounted for in all calculations

Table 2) are stored separately and later recombined during processing. That is, we do not use receiver phase cycling to perform the HN-TROSY line selection, nor do we store real and imaginary components of a dimension sequentially. This strategy was not only key in designing an HN-TROSY experiment with sensitivity-enhancement, but it also enabled implementing an efficient time-shared scheme, as described below. Tables 3 and 4 display the

Table 3 Combination of transients for sensitivity enhanced quadrature detection and line selection in HN-TROSY-NOESY spectra

Quadrature components	Transient combinations	Signal
R (t_1) R (t_2)	$A1_{xN} + A2_{xN} - A3_{xN} + A4_{xN}$	$S_N e^{(-i\omega_H t_3)} c_N^- c_{HN}^+$
I (t_1) R (t_2)	$-(A1_{yN} + A2_{yN} + A3_{yN} - A4_{yN})$	$S_N e^{(-i\omega_H t_3)} s_N^- c_{HN}^+$
R (t_1) I (t_2)	$A1_{yN} + A2_{yN} - A3_{yN} + A4_{yN}$	$S_N e^{(-i\omega_H t_3)} c_N^- s_{HN}^+$
I (t_1) I (t_2)	$A1_{xN} + A2_{xN} + A3_{xN} - A4_{xN}$	$S_N e^{(-i\omega_H t_3)} s_N^- s_{HN}^+$

S_N is the amplitude of the detected amide proton signal and ω_H is the frequency of the NOESY cross-peak encoded in the detected proton dimension (t_3). R & I refer to real and imaginary data for the respective evolution periods. The subscript N added to all transients emphasize that methyl signals have been eliminated (using the pulse phase ω_2, see above). The negative sign of the ^{15}N gyromagnetic ratio and $J_{NH} < 0$ was accounted for in all calculations

Table 4 Combination of transients for quadrature detection in HC-HSQC-NOESY spectra

Quadrature components	Transient combinations	Signal
R (t_1) R (t_2)	$A1_{xC}$–$A3_{xC}$	$S_c e^{(-i\omega_H t_3)} \cos(\omega_C t_1) \cos(\omega_{HC} t_2)$
I (t_1) R (t_2)	$-(A2_{yC}$–$A4_{yC})$	$S_c e^{(-i\omega_H t_3)} \sin(\omega_C t_1) \cos(\omega_{HC} t_2)$
R (t_1) I (t_2)	$A1_{yC}$–$A3_{yC}$	$S_c e^{(-i\omega_H t_3)} \cos(\omega_C t_1) \sin(\omega_{HC} t_2)$
I (t_1) I (t_2)	$A2_{xC}$–$A4_{xC}$	$S_c e^{(-i\omega_H t_3)} \sin(\omega_C t_1) \sin(\omega_{HC} t_2)$

S_C is the amplitude of the detected methyl proton signal and ω_H is the frequency of the NOESY cross-peak encoded in the detected dimension (t_3). R & I refer to real and imaginary data for the respective evolution periods. The subscript C added to all transients emphasize that amide signals have been eliminated (using the pulse phase ω_2, see above)

combinations of transients necessary to obtain the phase-sensitive HN-TROSY-NOESY and HC-HSQC-NOESY spectra, respectively.

Quadrature detection for the indirect dimensions of the ^{15}N-edited NOESY is performed in a manner similar to Echo-AntiEcho sensitivity-enhanced schemes. Real and imaginary components of the interferogram are obtained simultaneously, as can be seen in Table 2. In what follows, ^{15}N and ^{13}C pathways have been separated and the subscript N is added to the transient labels (e.g. $A1_{xN}$) to emphasize that only amide signals are being discussed. During processing, combinations of the transients provide real and imaginary components while simultaneously selecting for the slowly relaxing component of the HN multiplet (Table 3). Sensitivity enhancement in the amide spectrum can only be achieved by storing transients separately. Indeed, as seen in Table 3, all eight transients are used twice when performing quadrature detection; $A1_{xN}$, $A2_{xN}$, $A3_{xN}$ and $A4_{xN}$ are used to provide both the components $R(t_1)R(t_2)$ and $I(t_1)I(t_2)$. Likewise, $I(t_1)R(t_2)$ and $R(t_1)I(t_2)$ are obtained with $A1_{yN}$ through $A4_{yN}$. In a conventional NMR acquisition, phase cycling of the receiver is used to perform such combinations. However, the receiver would select either the combination providing $R(t_1)R(t_2)$ or that providing $I(t_1)I(t_2)$ (the same is true for $R(t_1)I(t_2)$ and $I(t_1)Rt_2)$). Quadrature detection and TROSY line selection can still be achieved but a total of 16 transients need to be acquired, although half of the data are redundant. This doubling in experimental time results in a $\sqrt{2}$ loss in sensitivity when compared to separate storage of transients. The same method has been used before to perform sensitivity-enhanced, Echo-AntiEcho quadrature detection with ST2-PT TROSY schemes (Brutscher et al. 1998; Zhu et al. 1999). As mentioned above, ST2-PT schemes lead to severe sensitivity losses in TS experiments (Würtz et al. 2007).

Frequency discrimination for the methyl proton indirect dimension cannot be achieved by conventional sequential acquisition of real and imaginary signal components. In a conventional ^{13}C-edited NOESY, hypercomplex data ($R(t_1)R(t_2)$, $I(t_1)R(t_2)$, $R(t_1)I(t_2)$, $I(t_1)I(t_2)$) would be obtained by varying the phases ω_1 or ω_2 for methyl carbons and ϕ_3 or ϕ_5 for methyl protons. However, the phases ϕ_3 and ϕ_5 have been set to provide sensitivity-enhanced quadrature detection and HN-TROSY line selection for the amide pathway, as discussed previously. To overcome this constraint, the real and imaginary components of the methyl proton dimension are acquired in a nested manner (Table 2) as dictated by the phases imposed by the amide protons. The appropriate pairing of the transients $A1_{xC}$–$A4_{xC}$ and $A1_{yC}$–$A4_{yC}$ (Table 4) resulting from such a nested acquisition provides hypercomplex data in the ^{13}C-edited NOESY (subscript C added to the transients to emphasize that only methyl signals are being discussed). Additionally, storing the transients separately was exploited to suppress artifacts in the ^{13}C-edited NOESY in a manner akin to phase cycling. The nested acquisition imposes that each component of the methyl proton dimension (R & I) be recorded twice. Since $A1_{xC}$–$A4_{xC}$ and $A1_{yC}$–$A4_{yC}$ can all be accessed during processing, various combinations can be used to retrieve real and imaginary components. Thus, the combinations shown in Table 3 can produce the $R(t_1)R(t_2)$, $I(t_1)R(t_2)$, $R(t_1)I(t_2)$, and $I(t_1)I(t_2)$ components not only for amide groups but also for methyl groups. However such a combination

results in artifacts in the ^{13}C-edited NOESY spectrum. These artifacts are suppressed if instead the combinations of Table 4 are employed. We exploited this advantage by reducing the size of traditional phase cycling in our experiment.

In summary, 16 transients stored separately ($A1_x$–$A4_x$ and $A1_y$–$A4_y$, each also recorded with opposite phases of ω_2) are efficiently used to (1) separate ^{15}N- and ^{13}C-dispersed spectra, (2) achieve sensitivity-enhanced quadrature detection in amide proton and nitrogen indirect dimensions, (3) perform TROSY line selection, (4) obtain quadrature detection in methyl proton and carbon indirect dimensions, and (5) suppress artifacts in ^{13}C edited NOESY. A single python script (available from the corresponding author upon request) separates ^{15}N and ^{13}C dispersed spectra, combines the transients according to Tables 3 and 4, and rearranges the data so that traditional NMRPipe (Delaglio et al. 1995) scripts can be used for processing (using the complex flag).

Demonstration on a 52 kDa monomeric protein

The critical impact of spectral resolution in NOESY experiments on the quality of NMR structures has been discussed thoroughly (Tikole et al. 2013). Here, we illustrate with selected examples the advantages of our newly developed 3D TS-HN-TROSY/HC-HSQC-NOESY (TS-TR/HS-NO) experiment over the existing TS NOESY experiment (Frueh et al. 2006) that features nOe correlations in the indirect dimension. For this comparison we used a TS-NOESY-HN-TROSY/HC-HSQC (TS-NO-TR/HS) (Frueh et al. 2006), updated with recent developments (supplementary information, S4), which provides a 3D NOESY-HN-TROSY (NO-TR) and a 3D NOESY-HC-HSQC (NO-HS) spectrum. Both TS experiments were acquired with the same number of points in all dimensions and within the same experimental time ($\sim$4 days). In what follows, only resolution is being considered; with our experimental conditions the TS-TR/HS-NO benefits from an improvement in sensitivity ($\sim$15 % in HN and $\sim$20 % in HC), over the TS-NO-TR/HS experiment (see supplementary information S5).

Figure 2a–d and a′–d′ compare H/H_{nOe} strips for a TS-NO-TR/HS and a TS-TR/HS-NO recorded at 600 MHz in the same time and for the same monomeric 52 kDa protein. The superior resolution of the nOe dimension in the TS-TR/HS-NO spectra (18.8 Hz/pt) reveals cross-peaks that are not resolved and hence undetected in the TS-NO-TR/HS (52 Hz/pt) spectra. Missing and erroneously assigned distance restraints drastically decrease the quality of structural models and may prevent determination of the proper fold (Nabuurs et al. 2006). Furthermore, in the TS-NO-TR/HS, the chemical shifts of signal maxima are

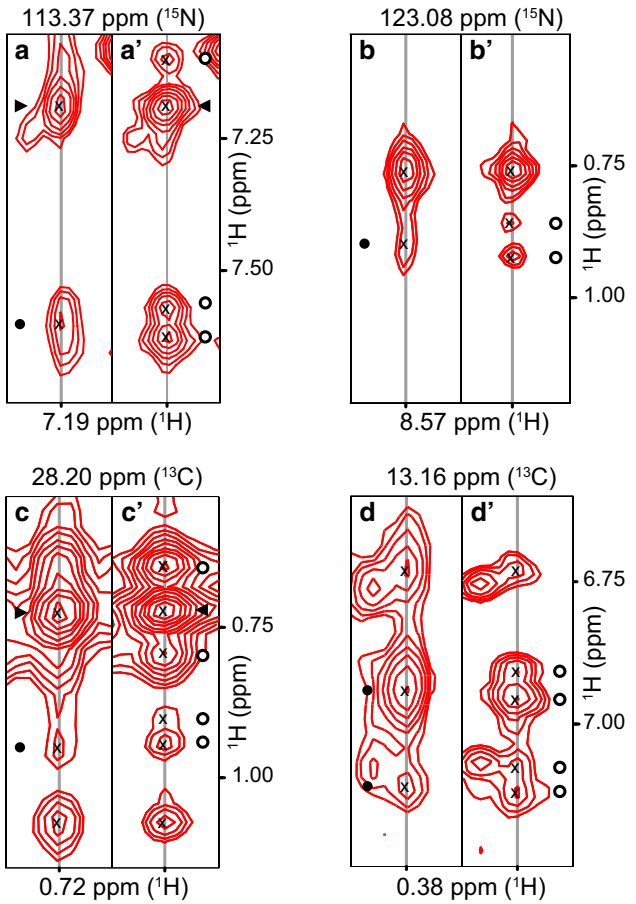

Fig. 2 Comparison of H/HnOe strips from TS-NO-TR/HS (**a**, **b**, **c**, **d**) and TS-TR/HS-NO (**a′**, **b′**, **c′**, **d′**) spectra. **a**, **a′** amide–amide and **b**, **b′** amide-methyl peaks in ^{15}N dispersed spectra. **c**, **c′** methyl–methyl and **d**, **d′** methyl-amide peaks in ^{13}C-dispersed spectra. X mark signal maxima. *Black filled circles* denote cross-peaks whose maxima are incorrectly identified in the TS-NO-TR/HS spectra. *Open circles* denote cross-peaks that are only resolved in the TS-TR/HS-NO spectra. *Triangles* mark diagonal peaks when applicable

shifted in the presence of overlap. As a result, these signals may be erroneously assigned. For example, the high resolution of the TR-NO in Fig. 2a′ reveals two cross-peaks below 7.5 ppm (open circles), each providing a distance restraint. Using the NO-TR spectrum (Fig. 2a) and comparing the chemical shifts of all amide protons picked in the spectrum with that of the single signal observed (black circle), one finds that the correct assignments (open circles) rank 7th and 10th. In this case, the NO-TR spectrum misses two correct distance restraints and instead produces one erroneous restraint. Similar examples are shown for amide-methyl (Fig. 2b, b′), methyl–methyl (Fig. 2c, c′) and methyl-amide (Fig. 2d, d′) cross-peaks. As a result, not only are the assignments provided by TS-NO-TR/HS spectra *incomplete* but also *erroneous*. Clearly, both the inability to resolve ambiguities and the risk of producing erroneous assignments is catastrophic in the context of

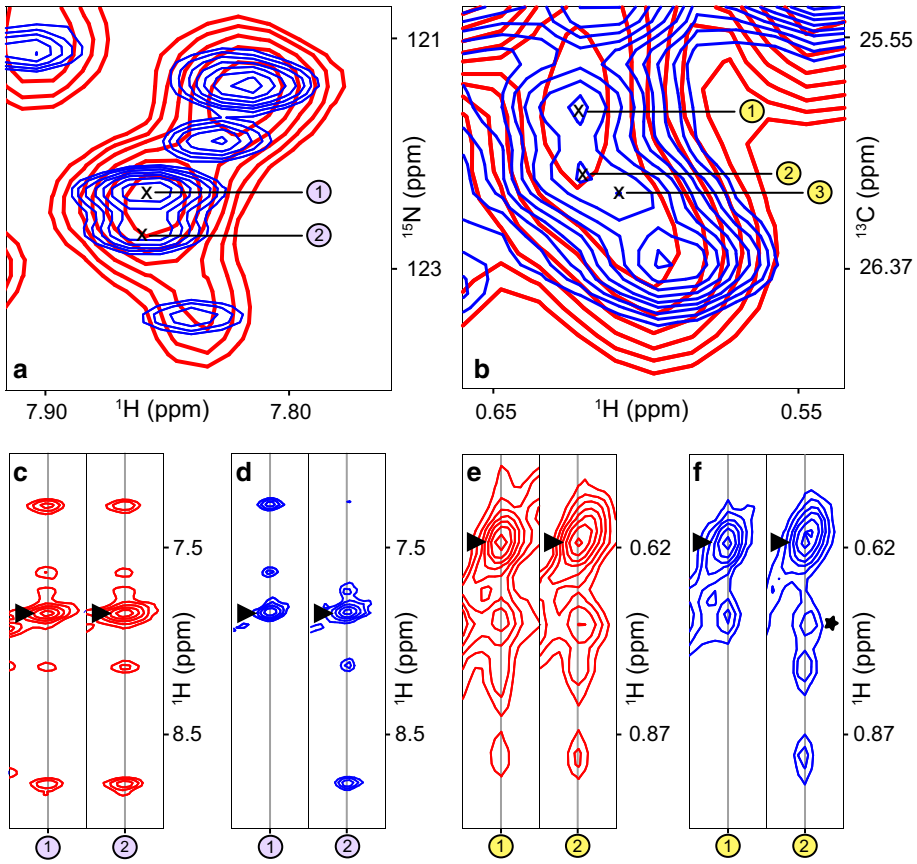

Fig. 3 TS-TR/HS-NO spectra from uniform (US, *red*) and non-uniform sampling (NUS, *blue*). **a** and **b** are overlays of US and NUS 2D projections of the indirect dimensions of 3D ^{15}N and ^{13}C dispersed spectra respectively. **c**, **d**, **e**, **f** H/HnOe strips centered on the signals labeled in the projections. nOe's can only be assigned appropriately in d and f. *Triangles* mark diagonal peaks. The *asterisk* marks a cross—peak that belongs to methyl peak 3

manual and automated nOe assignment procedures and consequently the structure determination process (Jee and Güntert 2003; Nabuurs et al. 2006). Indeed, automated peak picking resulted in at least 118 (^{15}N dispersed) and 127 (^{13}C dispersed) additional peaks when TS-TR/HS-NO was used in place of TS-NO-TR/HS. Here the threshold for peak picking was adjusted to compensate for differences in signal intensity, so these numbers reflect only the ability to resolve peaks (supplementary information S6). As discussed above, the differences between these numbers not only reflect missing correlations but also correlations for which assignment may be erroneous. Thus, the TS-TR/HS-NO spectra critically alleviate the shortcomings of the TS-NO-TR/HS when used in the NMR structure determination of large proteins.

The TS-TR/HS-NO experiment can be paired with non-uniform sampling (NUS) to provide spectra with high resolution in all dimensions. NUS accelerates data acquisition by recording only a subset of evolution times in indirect dimensions (quantified by a so called-sampling factor) instead of measuring all evolution times (Barna et al. 1987; Orekhov et al. 2003; Rovnyak et al. 2004; Marion 2006; Coggins et al. 2010; Kazimierczuk and Orekhov 2011; Holland et al. 2011; Maciejewski et al. 2012; Hyberts et al. 2012). For large proteins, this acceleration is exploited to maximize the resolution that can be obtained within a given spectrometer time and hence minimize signal overlap. The complete dataset is recovered using special reconstruction techniques (Barna et al. 1987; Orekhov et al. 2003; Rovnyak et al. 2004; Marion 2006; Coggins et al. 2010; Kazimierczuk and Orekhov 2011; Holland et al. 2011; Maciejewski et al. 2012; Hyberts et al. 2012). The quality of the reconstructed spectrum depends on the interplay between the sampling factor and the sparsity of signals present in indirect dimensions; spectra with fewer signals can tolerate lower sampling factors (Hyberts et al. 2014). Within this framework, the TS-TR/HS-NO has at least two advantages over the TS-NO-TR/HS. First and foremost, for the same resolution and acquisition time, the sampling factor is effectively doubled in the TS-TR/HS-NO. The spectral width of the indirect proton dimension in TS-NO-TR/HS must encompass both amide *and* methyl proton chemical shifts (here 13 ppm) and hence must be twice as big as that of TS-TR/HS-NO, which only needs to encompass the largest spectral width i.e. *either* methyl or amide protons (usually amides, here 6.5 ppm). Second, since NOESY cross-peaks appear in the detected dimension, fewer signals must be reconstructed in the indirect dimensions of TS-TR/HS-NO, so sparsity is increased. Although the improvements provided by using

the TS-TR/HS-NO experiment will depend on the method used for the reconstruction, all methods are expected to perform better with a higher sampling density and fewer signals to reconstruct (Orekhov and Jaravine 2011; Hyberts et al. 2014).

The improvement provided by non-uniform sampling was verified with an NUS-TS-TR/HS-NO spectrum acquired in the same experimental time as that used for conventional uniform acquisition (~4 days). A schedule of 4,500 complex points spanning 300 (^{1}H) × 150 (^{15}N) = 45,000 complex points was generated with the software package Poisson gap (10 % sampling factor) (Hyberts et al. 2012). Spectral reconstruction was performed with the iterative soft thresholding technique (Hyberts et al. 2012). Figure 3 highlights the advantages of increased resolution in the indirect dimensions within the context of NOESY cross-peaks assignment. In Fig. 3a, two (H, N) correlations (labeled 1 and 2) are separated by 0.001 ppm in ^{1}H and 0.314 ppm in ^{15}N. Without NUS the two corresponding H/H_{nOe} strips both feature the same five correlations (Fig. 3c). The increased resolution in the NUS spectrum reveals that only two cross-peaks belong to the first (H, N) correlation while the other three belong to the second (Fig. 3d). Likewise, with conventional acquisition, three NOESY cross-peaks can each be assigned to either of two (H, C) correlations (Fig. 2b, e), which are separated by 0.001 ppm in ^{1}H and 0.223 ppm in ^{13}C. Increased resolution in the NUS spectrum permits unambiguous assignment of these cross-peaks. Incidentally, the cross-peak marked with an asterisk belongs to a third correlation (Fig. 3b, labeled 3) and could only be discerned in the NUS spectrum (Fig. 3f). Automated peak picking of NOESY cross-peaks in NUS-TS-TR/HS-NO, provides at least 74 (^{15}N dispersed) and 41 (^{13}C dispersed) additional peaks when compared to the conventional acquisition (S6). The increased accuracy and completeness of automated peak picking that was facilitated in the NUS spectrum will translate into more reliable automated structure determination (Tikole et al. 2013).

Conclusion

We have developed an NMR experiment that enables more accurate and complete assignment of NOESY cross-peaks in large proteins. The experiment provides maximal digital resolution within a realistic acquisition time for amide–amide, amide-methyl, methyl–methyl and methyl-amide nOe correlations in a single experiment. The novel HN-TROSY scheme allowed implementing the TS strategy with superior sensitivity over sequential acquisition of both spectra. The reduced experimental time is particularly beneficial for data acquisition on short-lived, expensive protein samples. While this experiment was demonstrated on an ILV sample, it can also be used when methyl groups of other residues are labelled as ^{13}C–^{1}H (e.g. Ala, Thr, Met) (Gelis et al. 2007; Isaacson et al. 2007; Ayala et al. 2009; Sinha et al. 2011), provided the carbon adjacent to the methyl groups are not enriched in ^{13}C. At 600 MHz, our experiment provides at least a 2.8-fold increase in resolution along the nOe dimension over traditionally used NO-TR/HS experiments and improves both interactive and automated nOe assignment procedures. The experiment can be modified to suppress diagonal signals in the TR-NO spectrum as described by Meissner et al. (Meissner and Sørensen 2000), albeit with sensitivity losses in both TR-NO and HS-NO spectra. The full potential of our experiment was harnessed by implementing NUS along the indirect dimensions. The combined use of TS and NUS techniques provided in 4 days a pair of spectra that would otherwise require 80 days of spectrometer time. The resulting spectra possess optimal resolution in all dimensions and resolve ambiguities in assigning distance restraints. The TS-TROSY/HSQC-NOESY experiment will both facilitate the structure determination of large proteins and improve their accuracy, further increasing the molecular weight of monomeric proteins amenable for NMR structural studies.

Acknowledgments This work was supported by NIH, Grant R01-GM104257.

References

Ayala I, Sounier R, Usé N et al (2009) An efficient protocol for the complete incorporation of methyl-protonated alanine in perdeuterated protein. J Biomol NMR 43:111–119. doi:10.1007/s10858-008-9294-7

Barna JCJ, Laue ED, Mayger MR et al (1987) Exponential sampling, an alternative method for sampling in two-dimensional NMR experiments. J Magn Reson 77:69–77

Bodenhausen G, Ruben DJ (1980) Natural abundance nitrogen-15 NMR by enhanced heteronuclear spectroscopy. Chem Phys Lett 69:185–189

Boelens R, Burgering M, Fogh RH, Kaptein R (1994) Time-saving methods for heteronuclear multidimensional NMR of ((13)C, (15)N) doubly labeled proteins. J Biomol NMR 4:201–213. doi:10.1007/BF00175248

Brutscher B, Pardi A, Marion D (1998) Improved sensitivity and resolution in 1 H-13 C NMR experiments of RNA. J Am Chem Soc 120:11845–11851

Cai M, Huang Y, Sakaguchi K et al (1998) An efficient and cost-effective isotope labeling protocol for proteins expressed in *Escherichia coli*. J Biomol NMR 11:97–102

Coggins BE, Venters RA, Zhou P (2010) Radial sampling for fast NMR: concepts and practices over three decades. Prog Nucl Magn Reson Spectrosc 57:381–419. doi:10.1016/j.pnmrs.2010.07.001

Delaglio F, Grzesiek S, Vuister GW et al (1995) NMRPipe: a multidimensional spectral processing system based on UNIX pipes. J Biomol NMR 6:277–293

Farmer BT II (1991) Simultaneous[13C,15 N]-HMQC, a pseudo-triple-resonance experiment. J Magn Reson 93:635–641

Frueh DP, Vosburg DA, Walsh CT, Wagner G (2006) Determination of all nOes in 1H-13C-Me-ILV-U-2H-15 N proteins with two time-shared experiments. J Biomol NMR 34:31–40. doi:10.1007/s10858-005-5338-4

Gardner KH, Kay LE (1998) The use of 2H, 13C, 15N multidimensional NMR to study the structure and dynamics of proteins. Annu Rev Biophys Biomol Struct 27:357–406. doi:10.1146/annurev.biophys.27.1.357

Gelis I, Bonvin AMJJ, Keramisanou D et al (2007) Structural basis for signal sequence recognition by the 204-kDa translocase motor SecA determined by NMR. Cell 131:756–769

Goto NK, Kay LE (2000) New developments in isotope labeling strategies for protein solution NMR spectroscopy. Curr Opin Struct Biol 10:585–592

Goto NK, Gardner KH, Mueller GA et al (1999) A robust and cost-effective method for the production of Val, Leu, Ile (δ1). J Biomol NMR 13:369–374

Gross JD, Gelev VM, Wagner G (2003) A sensitive and robust method for obtaining intermolecular NOEs between side chains in large protein complexes. J Biomol NMR 25(3):235–242

Guo C, Tugarinov V (2009) Identification of HN-methyl NOEs in large proteins using simultaneous amide-methyl TROSY-based detection. J Biomol NMR 43:21–30. doi:10.1007/s10858-008-9285-8

Holland DJ, Bostock MJ, Gladden LF, Nietlispach D (2011) Fast multidimensional NMR spectroscopy using compressed sensing. Angew Chem Int Ed Engl 50:6548–6551. doi:10.1002/anie.201100440

Hyberts SG, Milbradt AG, Wagner AB et al (2012) Application of iterative soft thresholding for fast reconstruction of NMR data non-uniformly sampled with multidimensional Poisson Gap scheduling. J Biomol NMR 52:315–327. doi:10.1007/s10858-012-9611-z

Hyberts SG, Arthanari H, Robson SA, Wagner G (2014) Perspectives in magnetic resonance: NMR in the post-FFT era. J Magn Reson 241:60–73. doi:10.1016/j.jmr.2013.11.014

Isaacson RL, Simpson PJ, Liu M et al (2007) A new labeling method for methyl transverse relaxation-optimized spectroscopy NMR spectra of alanine residues. J Am Chem Soc 129:15428–15429. doi:10.1021/ja0761784

Jee J, Güntert P (2003) Influence of the completeness of chemical shift assignments on NMR structures obtained with automated NOE assignment. J Struct Funct Genomics 4:179–189

Kazimierczuk K, Orekhov VY (2011) Accelerated NMR spectroscopy by using compressed sensing. Angew Chem Int Ed Engl 50:5556–5559. doi:10.1002/anie.201100370

Keating TA, Miller DA, Walsh CT (2000) Expression, purification, and characterization of HMWP2, a 229 kDa, six domain protein subunit of Yersiniabactin synthetase. Biochemistry 39:4729–4739

Keller RLJ (2003) The CARA/Lua programmers manual

Maciejewski MW, Mobli M, Schuyler AD et al (2012) Data sampling in multidimensional NMR: Fundamentals and strategies. In: Billiter M, Orekhov V (eds) Novel sampling approaches in higher dimensional NMR: Top Curr Chem, vol 316. Springer, Berlin, pp 49–77. doi:10.1007/128

Marion D (2006) Processing of ND NMR spectra sampled in polar coordinates: a simple Fourier transform instead of a reconstruction. J Biomol NMR 36:45–54. doi:10.1007/s10858-006-9066-1

Marion D, Wuthrich K (1983) Application of phase sensitive two-dimensional correlated spectroscopy (cosy) for measurements of 1H-1H spin-spin coupling constants in proteins. Biochem Biophys Res Commun 113:967–974

Meissner A, Sørensen OW (2000) Three-dimensional protein NMR TROSY-type 15 N-resolved 1 HN–1 HN NOESY spectra with diagonal peak suppression. J Magn Reson 142:195–198

Muchmore DC, McIntosh LP, Russell CB, Anderson DE, Dahlquist FW (1989) Expression and nitrogen-15 labeling of proteins for proton and nitrogen-15 nuclear magnetic resonance. In: Norman JO, Thomas LJ (eds) Methods in enzymology, vol 177. Academic Press, pp 44–73. doi: 10.1016/0076-6879(10)77005-1

Nabuurs SB, Spronk CAEM, Vuister GW, Vriend G (2006) Traditional biomolecular structure determination by NMR spectroscopy allows for major errors. PLoS Comput Biol 2:e9. doi:10.1371/journal.pcbi.0020009

Nietlispach D (2005) Suppression of anti-TROSY lines in a sensitivity enhanced gradient selection TROSY scheme. J Biomol NMR 31:161–166. doi:10.1007/s10858-004-8195-7

Orekhov VY, Jaravine VA (2011) Analysis of non-uniformly sampled spectra with multi-dimensional decomposition. Prog Nucl Magn Reson Spectrosc 59:271–292. doi:10.1016/j.pnmrs.2011.02.002

Orekhov VY, Ibraghimov I, Billeter M (2003) Optimizing resolution in multidimensional NMR by three-way decomposition. J Biomol NMR 27:165–173

Pervushin K, Riek R, Wider G, Wüthrich K (1997) Attenuated T2 relaxation by mutual cancellation of dipole–dipole coupling and chemical shift anisotropy indicates an avenue to NMR structures of very large biological macromolecules in solution. Proc Natl Acad Sci USA 94:12366–12371

Pervushin KV, Wider G, Wüthrich K (1998) Single transition-to-single transition polarization transfer (ST2-PT) in [15 N,1H]-TROSY. J Biomol NMR 12:345–348. doi:10.1023/A:1008268930690

Piotto M, Saudek V, Sklenár V (1992) Gradient-tailored excitation for single-quantum NMR spectroscopy of aqueous solutions. J Biomol NMR 2:661–665

Roehrl MHA, Heffron GJ, Wagner G (2005) Correspondence between spin-dynamic phases and pulse program phases of NMR spectrometers. J Magn Reson 174:325–330. doi:10.1016/j.jmr.2005.02.001

Rovnyak D, Frueh DP, Sastry M et al (2004) Accelerated acquisition of high resolution triple-resonance spectra using non-uniform sampling and maximum entropy reconstruction. J Magn Reson 170:15–21. doi:10.1016/j.jmr.2004.05.016

Sattler M, Maurer M, Schleucher J, Griesinger C (1995) A simultaneous (15)N, (1)H- and (13)C, (1)H-HSQC with sensitivity enhancement and a heteronuclear gradient echo. J Biomol NMR 5:97–102. doi:10.1007/BF00227475

Shaka AJ, Reeler J, Frenkiel T, Freeman RAY (1983) An improved sequence for broadband decoupling: WALTZ-16. J Magn Reson 52:335–338

Sinha K, Jen-Jacobson L, Rule GS (2011) Specific labeling of threonine methyl groups for NMR studies of protein–nucleic acid complexes. Biochemistry 50:10189–10191. doi:10.1021/bi201496d

Tikole S, Jaravine V, Orekhov VY, Güntert P (2013) Effects of NMR spectral resolution on protein structure calculation. PLoS ONE 8:e68567. doi:10.1371/journal.pone.0068567

Van Ingen H, Vuister GW, Tessari M (2002) A two-dimensional artifact from asynchronous decoupling. J Magn Reson 156:258–261. doi:10.1006/jmre.2002.2564

Würtz P, Aitio O, Hellman M, Permi P (2007) Simultaneous detection of amide and methyl correlations using a time shared NMR experiment: application to binding epitope mapping. J Biomol NMR 39:97–105. doi:10.1007/s10858-007-9178-2

Yang D, Kay LE (1999) Improved 1HN-detected triple resonance TROSY-based experiments. J Biomol NMR 13:3–10. doi:10.1023/A:1008329230975

Zhu G, Xia Y, Sze KH, Yan X (1999) 2D and 3D TROSY-enhanced NOESY of 15 N labeled proteins. J Biomol NMR 14:377–381